Published in final edited form as:
Pharm Res. 2013 March ; 30(3): 878–888. doi:10.1007/s11095-012-0929-8.

^{89}Zr-Labeled Paramagnetic Octreotide-Liposomes for PET-MR Imaging of Cancer

Diane S. Abou,
Molecular Pharmacology and Chemistry Program, Memorial Sloan-Kettering Cancer Center, 1275 York Avenue, Box 16, New York, New York 10065, USA

Daniel L. J. Thorek,
Molecular Pharmacology and Chemistry Program, Memorial Sloan-Kettering Cancer Center, 1275 York Avenue, Box 16, New York, New York 10065, USA

Nicholas N. Ramos,
Molecular Pharmacology and Chemistry Program, Memorial Sloan-Kettering Cancer Center, 1275 York Avenue, Box 16, New York, New York 10065, USA

Martijn W. H. Pinkse,
Analytical Biotechnology, Department Biotechnology, TU Delft, Julianalaan 67, 2628 BC Delft, Netherlands

Hubert T. Wolterbeek,
Radiation and Isotopes for Health, Department of Radiation, Radionuclides & Reactor, TU Delft, Mekelweg 15, 2629 JB Delft, Netherlands

Sean D. Carlin,
Radiochemistry & Imaging Sciences Service, Department of Radiology, Memorial Sloan-Kettering Cancer Center, 1275 York Avenue, Box 16, New York, New York 10065, USA

Bradley J. Beattie, and
Department of Medical Physics, Memorial Sloan-Kettering Cancer Center, 1275 York Avenue, Box 16, New York, New York 10065, USA

Jason S. Lewis
Molecular Pharmacology and Chemistry Program, Memorial Sloan-Kettering Cancer Center, 1275 York Avenue, Box 16, New York, New York 10065, USA

Radiochemistry & Imaging Sciences Service, Department of Radiology, Memorial Sloan-Kettering Cancer Center, 1275 York Avenue, Box 16, New York, New York 10065, USA

Jason S. Lewis: lewisj2@mskcc.org

Abstract

Purpose—Dual-modality PET/MR platforms add a new dimension to patient diagnosis with high resolution, functional, and anatomical imaging. The full potential of this emerging hybrid modality could be realized by using a corresponding dual-modality probe. Here, we report pegylated liposome (LP) formulations, housing a MR T_1 contrast agent (Gd) and the positron-emitting ^{89}Zr (half-life: 3.27 days), for simultaneous PET and MR tumor imaging capabilities.

Correspondence to: Jason S. Lewis, lewisj2@mskcc.org.

Electronic supplementary material The online version of this article (doi:10.1007/s11095-012-0929-8) contains supplementary material, which is available to authorized users.

Methods—^{89}Zr oxophilicity was unexpectedly found advantageous for direct radiolabeling of preformed paramagnetic LPs. LPs were conjugated with octreotide to selectively target neuroendocrine tumors *via* human somatostatin receptor subtype 2 (SSTr2). ^{89}Zr-Gd-LPs and octreotide-conjugated homolog were physically, chemically and biologically characterized.

Results—^{89}Zr-LPs showed reasonable stability over serum proteins and chelator challenges for proof-of-concept *in vitro* and *in vivo* investigations. Nuclear and paramagnetic tracking quantified superior SSTr2-recognition of octreotide-LP compared to controls.

Conclusions—This study demonstrated SSTr2-targeting specificity along with direct chelator-free ^{89}Zr-labeling of LPs and dual PET/MR imaging properties.

Keywords

nanoparticles; octreotide; PET-MRI; targeted molecular imaging; ^{89}Zr

INTRODUCTION

Personalized medicine has the potential to improve patient care by providing specific diagnostic and treatment solutions. This shift in medical practice is being driven by molecular imaging tools that enable detection of disease, monitoring of personalized therapy and optimization of treatment strategy. In radiology, hybrid imaging systems such as PET/CT and SPECT/CT have revolutionized patient management, enabling high spatial resolution and sensitivity of detection overlaid with anatomically relevant information. However, CT scans provide poor soft tissue contrast and radiation exposure (1).

The recent convergence of PET and MR platforms enables functional and anatomical data to be concurrently acquired with high sensitivity for non-invasive analysis of disease (2). PET imaging provides *in vivo* quantification of the radiotracer distribution, while MR offers anatomical localization through high-resolution imaging with excellent soft-tissue contrast. Gd paramagnetic contrast agents produce positive contrast using T_1-weighted image acquisition, and are included in nearly half of all MR studies (3,4). Nevertheless, the limited sensitivity of MR requires the delivery of high concentrations of paramagnetic material (5) as compared to nuclear imaging.

We hypothesized that a dual-modality paramagnetic radiopharmaceutical would be useful in realizing the full potential of this emerging hybrid modality. Namely, that a single probe carrying both a highly paramagnetic Gd-payload and a PET radionuclide could be designed using liposomal constructs. Utilization of a dual-modality probe could correct for imaging artefacts of one modality; improve delineation and characterization of metastasis in soft tissue by Gd contrast enhancement; and correct for partial volume effects in PET (6).

For molecular imaging, liposomes (LPs) have previously incorporated long-lived gamma emitters for low-resolution and non-quantitative SPECT (7). However, in this work PET is used to quantitatively assess targeted-LP distribution using ^{89}Zr for the first time. Zirconium-89 is a positron-emitter with a half-life of 3.27 days (8) which is suitable for *in vivo* tracking of long circulating PEG_{2000}-LP (Polyethylene Glycol) (9). Herein, we describe a unique and facile chemical method to prepare simultaneous paramagnetic and radiopharmaceutical probes. Unexpectedly, an advantage of ^{89}Zr is that chelator-free labeling can be achieved directly on paramagnetic LPs.

LPs can also confer selective tumor-targeting following antibody (10) or peptide functionalization (11,12). Here we have employed octreotide (OCT), a well-characterized peptide targeting human somatostatin receptor subtype 2 (SSTr2; IC_{50} 02.0±0.7 nM) (13), as

a model system. This validated targeting vector enables selective accumulation of LPs; however, OCT-LP (OL) has not been quantified *in vivo* (9,11,12,14). SSTr2 targeted and control ^{89}Zr-Gd-LPs (Scheme 1) were characterized and tested *in vitro* and *in vivo* in mouse models. To our knowledge, this is the first report of a LP-based probe fusing PET and MR contrast capabilities to image neuroendocrine tumors.

MATERIALS AND METHODS

Chemicals

DSPC (1,2-disearoyl-*sn*-glycero-3-phosphocholine) and DSPE-PEG$_{2000}$-OMe (1,2-distearoyl-*sn*-glycero-3-phosphoethanol-amine-N-[methoxy(polyethyleneglycol)-2000]) were purchased from Lipoid AG, Cham, Switzland; cholesterol and DSPE-PEG$_{2000}$–CO_2H (1,2-distearoyl-*sn*-glycero-3-phosphoethanol-amine-N–[carboxylic acid (polyethyleneglycol)-2000]) were purchased from Avanti polar Inc., Alabaster, AL, USA. Octreotide (OCT) was purchased from AnaSpec Inc., Fremont, CA. EDC (1-ethyl-3–[3-dimethylaminopropyl]carbodiimide hydrochloride), S-NHS (N-hydroxysulfosuccinimide); HEPES (N-2-hydroxyethylpiperazine-N′-2-ethanesulfonic acid) and zirconium(IV)-chloride (Zr) were purchased from Sigma-Aldrich. Gd-DTPA-BiSA (Gadolinium Diethylenetriaminepentaacetic acid bis-stearylamide) was purchased from Chemir Analytical Services, Maryland Heights, MO. Desferrioxamine mesylate (DFO) was purchased from Calbiochem, Merck KGaA, Darmstadt, DE.

^{89}Zr was produced by irradiating an ^{86}Y target. The target was washed with strong acids, and the resulting solution was purified using an hydroxamate gel column eluted with oxalic acid as described by Holland *et al.* (15) ^{89}Zr[Zr]-oxalate was the radioactive source used for radiolabeling.

OCT Coupling Procedure and Analysis

OCT (1 eq.) was coupled to DSPE-PEG$_{2000}$–CO_2H (1 eq.) using EDC (10 eq.) and S–NHS (5 eq.), in HEPES buffer (10 mM HEPES; 150 mM NaCl adjusted to pH 6) and stirred at room temperature for 20 h. The mixture was analyzed using HPLC (Shimadzu system equipped with a UV diode array detector) and LC-ESI-QTOF MS (Waters QT of Premier). A C4-reverse phase column (Alltech Prosphere HP C4 300 Å–5 μm, 150 mm*4.6 mm) was eluted with acidified ultrapure deionized water (0.01% TFA; 0.1% NH_4Cl) at a flow rate of 1 mL/min with an increasing linear gradient of methanol from 10 to 100% over 60 min. The column effluent was directly electrosprayed in ESI source. The mass spectrometer was set in the positive ion mode (ESI+) and acquired spectra from *m/z* 400 to 1500 Da at one scan rate per second (Fig. 1a, b).

LPs Preparations

Two formulations (octreotide-liposome—OL and control-liposome—CL) constituted of DSPC/cholesterol/Gd-DTPA-BiSA/DSPE-PEG$_{2000}$-OMe/DSPE-PEG$_{2000}$-CO_2H were prepared with the following ratio: 42/33/20/3/2. The sum of all compounds number of moles equaled 40 μmol/ animal injection. All chemicals were dissolved in a total volume of 6 mL with a dichloromethane / methanol mixture (1:1). The solution was vacuum-dried to get a thin lipidic film. The film was hydrated in HEPES buffer (pH 6), resulting in a milky suspension. Each mixture was extruded through polycarbonate membrane filters with 200 nm (ten times) and 100 nm (ten times) pores, using the Lipofast extruder (Avestin, Canada). While extruding, the temperature was maintained at 55°C. The extruded solution was ultracentrifuged 1 h, at 4°C, using a Beckman L7 ultracentrifuge at 266000*g*. The pellet was suspended in fresh HEPES buffer pH 6 (2 mL). This suspension was split in two equal volumes of 1 mL: CL and OL. For OL, EDC (105 mM, 6 μL per animal injection) and S-

NHS (50 mM, 6 μL per injection) were added 15 min prior to OCT addition (1 mM; 23 μL per injection). The conjugation was conducted overnight at 4°C with gentle shaking of the sample using a rotator. Then, OL and CL were washed and OL supernatant was HPLC analyzed to determine the amount of unbound OCT (Fig. 1d). OL and CL pellets were both suspended in 1 mL of fresh buffer (HEPES 10 mM; NaCl 150 mM; pH 7.4). Stewart assay quantified the lipid content of each sample (16). The average diameter and PDI of OL and CL were measured using dynamic light scattering (Malvern instrument, Westborough, Ma, USA).

Monolayer Study: Procedure and Equipment

Zr-chloride (Zr) and desferrioxamine mesylate (DFO) adsorption to lipid monolayers were tested using a Wilhelmy wire attached to a microbalance (TroughS, Kibron Inc., Helsinki, Finland) and analyzed with Delta Pi software (Fig. 2) (17). A well (2 cm diameter) filled with HEPES buffer pH 7.4 formed a meniscus with an air–water interface. 1 to 5 μL of DSPC dissolved in buffer (1 mg/mL) was incorporated on the meniscus to reconstitute a lipid monolayer film. Increasing DSPC addition resulted in increasing initial surface pressures (π_i). Varying π_i, we examined $\Delta\pi$ after addition of Zr (10 mM; 20 μL) in the aqueous compartment (Fig. 2b; $15 < \pi_i < 55$ mN.m^{-1}). $\Delta\pi$, the surface tension of the monolayer, was calculated by subtracting final surface pressure (π_f, post chemical addition) to initial surface pressure (π_i). π_f never exceeded the collapsing value of 65 mN/m, where the monolayer is disrupted (Fig. 2b) (18). In another trial (Fig. 2d), starting from a dense lipid packing, π_i =50 mN/m, the adsorption and desorption of Zr was observed upon addition of DFO. Finally, the reverse experiment was achieved by first adding DFO and then Zr (Fig. 2e).

LPs Radiolabeling

[^{89}Zr]Zr-oxalate (15) treated with aqua regia and dried (19) was dissolved in saline, resulting in [^{89}Zr]Zr-hydroxide chloride. LPs were incubated with the radioactive preparation either at room temperature or at 45°C for 2 h. The radiolabeled LPs were purified using size exclusion chromatography eluted with 10 μL of EDTA (50 mM) in HEPES buffer pH 7.4 (Sephadex G-25; gamma counted using Wizard 1480, Perkin Elmer, Waltham, MA, USA; Supplementary Material Fig. S1). The preparations for animal injection were concentrated by centrifugation (3 cycles of 1811*g*; 15 min; centrifuge Eppendorf-5810R) using Millipore Centriprep YM-10 Centrifugal units. A final filtration was performed to sterilize the preparations using Millipore syringe filter with 200 μm porosity.

The specific activity was calculated after LPs purification either considering the activity (μCi) per lipids (mol) after Stewart assay (16) or the activity per LPs particle (following Enoch approximation of lipids per LPs) (20).

The number of lipid molecules per ^{89}Zr atom was calculated. The lipid molecule number (N) was found accordingly to: N = mole number · N_A (Avogadro's Number). The lipid ratio used for this formulation was: Total mol lipids = 0.89 DSPC[mol] + 0.064 DSPE – PEG_{2000} – CO_2H[mol] + 0.046 DSPE – PEG_{2000} – OMe[mol].

^{89}Zr atom number (N) was calculated as followed: $A=\lambda . N$

Where A = Activity (disintegration per second); $\lambda = Ln(2) / T_{1/2}$; $T_{1/2}$ = Half-life of ^{89}Zr (second); $T_{1/2}$ (^{89}Zr)=78.4 h=282240 s.

Stability Study

^{89}Zr-CL was incubated overnight at 37°C in HEPES buffer pH 7.4 and split in three groups of wash (Millipore Centriprep YM-10). ^{89}Zr-CL was washed with EDTA (5 mM) or PBS (137 mM NaCl; 2.7 mM KCl; 10 mM $Na_2HPO_4.2H_2O$; 2 mM K_2HPO_4; pH=7.4) or HEPES buffer (pH=7.4). In another trial, ^{89}Zr-CL was incubated in bovine serum albumin (BSA) (5%w/v; 100 μL; 1:1; v/v with 75 mM lipids) and mouse serum protein (MSP) (100 μL; 1:1 v/v with 75 mM lipids) at various time points (24, 48 and 96 h, $n \geq 2$) at 37°C. LPs were separated from serum proteins using Sepharose 4B gel column (Fig. 3a). The protein content of each fractions (1 mL) was titrated using the Pierce® BCA protein assay (Pierce, Thermo Scientific). The fractions were gamma counted and these data were charted in the radioactive stability profile (Fig. 3b).

In Vitro Evaluation

In vitro experiments were undertaken using C6 human somatostatin receptor type 2 (SSTr2-postive) transduced glioblastoma cells (21). The cells were grown at 37°C and 5% CO_2 in DMEM supplemented with 10% fetal calf serum with 1% penicillin and streptomycin. ^{89}Zr-OL; CL (320 nmol of lipids / 0.464 nmol octreotide for OL per 1×10^6 SSTr2-postive cell line) and OL blocked with octreotide (0.1 nmol / vial) were incubated for 0.5; 1; 2 h (n=3; SEM). The cell suspensions were spun down and washed twice with HEPES buffer pH 7.4. The suspensions were analyzed by gamma and cell counting (Supplementary Material Fig. S2).

Imaging Protocols and Co-registration

Animal experiments were conducted according to National Institute of Health (NIH) guidelines and the Institutional Animal Care and Use Committee of MSKCC. Female Nu/Nu NCRNU mice were subcutaneously inoculated with 1.5×10^6 cells on each shoulder with wild type (left) and SSTr2-postive transduced cell (right). Tumors were allowed to grow 15 days, reaching an average size of 25–30 mm^3 (as calculated: $V = 0.5 \times (\text{length} \times \text{width}^2)$ (22) where length and width were measured using MR scans. PET and MR were acquired on 5 animals after injections of OL and CL with the following amounts per injection: 35–40 μCi ^{89}Zr; 2.78 μmol Gd-DTPA-BiSA; 6.53 μmol lipids; and 6.53 nmol OCT for OL.

PET Imaging—The mice were scanned 30 to 45 min on a micro-PET Focus 120 scanner (Siemens) at 4, 10, 24 and 48 h post injection (p.i.), under inhalation of 1% isoflurane (Baxter Health-care, Deerfield, IL, USA) / oxygen gas mixture (flow rate: 2 L/min) for anesthesia. PET scans were reconstructed using Concorde Microsystems software.

MR Acquisition—MR was conducted on each animal at 24 and 50 h p.i. T_1-weighted images were acquired on a Bruker 4.7 T 40 cm bore scanner equipped with 400 mT/m shielded gradients (Bruker Biospin MRI GmbH, Ettlingen, Germany). A 36-mm ID quadrature resonator (Stark Contrast MRI Coils Research Inc., Erlangen, Germany) was used for excitation and detection. A deionized water phantom was placed next to the mouse body as a reference for signal intensity. Initial T_2 scout images were acquired along 3 orientations for tumor localization. Axial gradient-echo images were then acquired across the xenograft tumor and the water phantom with the following acquisition parameters: TR (Repetition Time) 61 ms, TE (Echo Time) 2 ms, 1 mm slice thickness, 182 × 188 mm in-plane resolution, 16 averages. A total of 5 slices were imaged. MR co-registered 3D T1-weighted images were acquired with TR 61 ms, TE 2 ms, spatial resolution of 350 mm, and 4 averages. The tumor contrast was measured using Image J software (NIH; Bethesda, MD) looking at the grayscale intensity of group-blind region of interest (ROI) measurements. The

normalized contrast enhancement was calculated by subtracting pre-injection (*pre*) to post-injection (*post*) tumor over water ROI ratio (a).

$$\%\ \text{Enhancement} = \left[\left[\frac{\text{ROI Tumor}}{\text{ROI Water}}\right]\text{Post} - \left[\frac{\text{ROI Tumor}}{\text{ROI Water}}\right]\text{Pre}\right] * 100 \quad \text{(a)}$$

Co-registration—One animal of each liposome group was submitted to CT-PET-MR co-registration. CT scans were acquired on the mouse 10 min using a microCAT II, manufactured by Imtek, Inc (Oak Ridge, TN). Accurate PET to MR registration was made possible by immobilizing the mouse on a movable PET, CT and MR compatible bed using a thin plastic wrap. The mouse was maintained in a single rigid position under isoflurane anesthesia during and between PET, CT and MR imaging sessions. Because PET and CT scanners both used calibrated bed positioning systems, the registration transformation between these two modalities could be determined *a priori* (23). Our MR scanner does not have a similar bed positioning capability, therefore MR to PET or MR to CT registrations require information contained within the MR images. Retrospective mutual information registration algorithms work efficiently in registering MR to CT data based on the bone visualization. Therefore, for the datasets described, we used this approach plus the *a priori* determined CT to PET rigid-body transform to achieve the MR to PET registration.

After imaging completion, organs and tumors were collected and gamma counted. Bones, epiphysis and the marrow were separated and gamma counted (19).

Statistical Analysis

The statistical difference in tumor uptake was analyzed using a one-tailed unpaired student's *t*-test for comparing SSTr2-postive tumor uptake of OL *versus* CL; and, a one-tailed paired student's *t*-test for OL SSTr2-positive and control wild type tumor.

RESULTS

Coupling of OCT to DSPE-PEG_{2000}-CO_2H and PEG_{2000}-LPs

OCT was first coupled in solution to DSPE-PEG_{2000}-CO_2H using EDC and S-NHS at pH 6 to selectively react at the peptide's N-terminus (24). The lipid-PEG_{2000}-OCT conjugate was identified using mass spectrometry (Fig. 1b). This reaction was then achieved on preformed LPs (Scheme 1) (25). Coupling was performed without a peptide-protecting group to abrogate a potentially difficult deprotection step, which could be destructive to LPs. Coupling efficiency on LPs was 70% (Fig. 1d), yielding targeted paramagnetic Gd-OL.

Octreotide-Liposomes (OL) and Control-Liposomes (CL) were identified with similar diameters of 115±2 nm, similar narrow polydispersity index (PDI) of 0.04±0.01 and, as previously reported, similar zeta potentials (11). The ratio of OCT to lipid (mol/mol) in the OL preparation was calculated to be 0.001. According to the Enoch method (20), a LP of 115 nm diameter is therefore composed of ~85700 lipid molecules, ~40809 Gd chelates (Gd-DTPA-Bistearylamide) molecules and ~85–90 molecules of OCT.

Zr Adsorption Into DSPC (1,2-distearoyl-*sn*-glycero-3-phosphocholine) Membrane

The chelate desferrioxamine (DFO) has been used to radiolabel antibodies with ^{89}Zr (8,26). We discovered that this approach, in the context of a bilayered lipid particle, was plagued by interaction of the radiometal with the lipids' phosphate head groups (Fig. 2a). This metal–lipid affinity presented the opportunity to radiolabel LP in a chelator-free strategy.

To verify this hypothesis, we tested Zr adsorption to a DSPC lipid monolayer (Fig. 2c #1). The exponential increase in membrane surface tension ($\Delta\pi$) when supplementing Zr proved its adsorption, even when the lipid compression was high (Fig. 2b). It suggested a strong Zr affinity for the stacked lipid phosphate heads of membranes (27).

After saturating the membrane and the aqueous compartment with Zr (Fig. 2d #2), Zr desorption was attempted by DFO chelation. The first μmol of DFO added chelated Zr suspended in the water layer (Fig. 2d #3) resulting in no membrane interaction ($\Delta\pi=0$). Then, even though lipids were in excess, DFO finally desorbed Zr ($\Delta\pi<0$; Fig. 2d #4). In a different experiment (Fig. 2e), DFO was first adsorbed onto the monolayer (#1) and it was then desorbed as a metal-complex (#4). Zr-DFO desorption showed the superior complexing power of DFO against lipids.

As discussed further, radiolabeling of LP through DFO chelation was however not the chosen strategy because of DFO strong hydrophilic affinity for the monolayer. Instead, Zr oxophilicity was exploited to radiolabel LPs membranes through phosphate affinity with lipids polar heads.

LP Radiolabeling and Stability Assays

Gd-LPs were radiolabeled using ^{89}Zr adsorption, and the resulting preparation was purified and tested with stability assays. No significant difference of labeling efficiency was found between OL and CL, showing the negligible effect of OCT on LP surfaces.

Radiolabeling conducted at 45°C was more successful than that at room temperature (Supplementary Material Fig. S1a). At 45°C, the efficiency approached 99% when low amounts of lipid and radioactivity were used. This efficiency decreased exponentially with increasing lipid concentration (Supplementary Material Fig. S1b). High lipid concentration correlated with high LPs' density in solution and low radiolabeling efficiency. Moreover, the diameter and poly dispersity index of ^{89}Zr-LPs remained unchanged after labeling and purification. For the optimized preparation used for *in vitro* and *in vivo* studies, the specific activity was calculated to be 9.82 μCi / mg of total lipid or (5.2×10^{-19}Ci per LP). The number of DSPC molecules was 3.215×10^{12} per ^{89}Zr atom. The number of DSPE-PEG$_{2000}$-CO_2H molecules was 2.31×10^{11} per ^{89}Zr atom and for DSPE-PEG$_{2000}$-OMe the number of molecules was 1.52×10^{11} per ^{89}Zr atom.

Challenging ^{89}Zr-CL with EDTA (5 mM) resulted in 40 ±3.5% of total radioactivity associated to LPs and 87±1.4% when washed with PBS (phosphate challenge). This contrasted with no loss of radioactivity when washed with HEPES buffer at pH 7.4. LPs incubation in bovine serum albumin (BSA) (5%w/v) or mouse serum proteins (MSP) demonstrated a moderate stability (Fig. 3a, b). After 24 h and up to 96 h of incubation, approximately 50% of the radioactivity remained bound to LPs at 37°C. These results underscore that, in the absence of a chelator, ^{89}Zr binding to LPs is stable enough to track vesicle constructs *in vitro* and *in vivo*.

In Vitro Experiments

The affinity of ^{89}Zr-labeled OL for its target was tested *in vitro* and validated using a transduced SSTr2-positive cell line (Supplementary Material Fig. S2) (21). OL showed significantly greater ($p<0.05$) accumulation to SSTr2 expressing cells as compared to that of CL. In addition, OL was selectively blocked through the addition of excess OCT.

Imaging and PET-MR Co-registration

OL and CL were then studied using MR (Fig. 4) and PET (Fig. 5) imaging in the context of a dual-xenograft mouse model. Voxel-by-voxel analysis of MR acquisitions 50 h p.i. (Fig. 2) reveals contrast enhancement (mean tumor ROI of 180) for SSTr2-postive tumor as compared to that of control tumors (mean of 139). However, little tumor contrast is observed between SSTr2 and control tumors for the CL injected mouse (127 and 145, respectively) close to the baseline mean values of 126 and 123. The % contrast enhancement relative to baseline shows an approximate 2-fold increase of signal for the SSTr2-tumors of OL injected mice as compared to CL (n=5), (Fig. 4c).

PET showed that the tumor radioactivity was predominantly driven by the high blood levels up to 24 h (4 h MIP, Supplementary Material Fig. S3) and the tumors' permeable vasculature (28), suggested by low tumor-to-blood ratios (Fig. 5d—24 h p.i.). Also, no specific SSTr2 recognition was observed at 24 h with Gd and ^{89}Zr tracking (Supplementary Material Fig. S5a, b). After 24 h, tumors were readily distinguishable from the blood-pool due to progressive clearance of the agent. At 50 h, OL targeting of SSTr2-positive tumors became apparent, in addition to the EPR effect (28) as seen with the autoradiography of the harvested tumors (Supplementary Material Fig. S4).

At 50 h p.i., OL tumor uptake values in SSTr2-positive tumors (3.5–5%ID/g) were significantly greater (p<0.05) than for the control (2.5–3%ID/g). Furthermore, OL SSTr2-positive tumor uptake exceeded CL in both wild type and SSTr2 tumor uptake with ~2%ID/g (Fig. 5b).

Activity in the liver and spleen showed LP clearance through the reticular endothelial system (RES), and not dissociated free ^{89}Zr (9,19). RES uptake reached a maximum of 18% ID/g (Fig. 5b). This is relatively low as compared to reported values of immuno-targeted LP in mice (10).

Bone accumulation was visualized using PET throughout the study (Supplementary Material Fig. S3). At 4 h only ~2%ID/g was observed, however bone uptake increased to 12%ID/g at later time points. No significant activity was found in the marrow, in agreement with reported studies of ^{89}Zr-hydroxide chloride localized in bone mineral (19). It is likely the exchange of ^{89}Zr from LP to serum proteins results in a final homing of ^{89}Zr-colloids to bone minerals.

The greatest tumor-to-muscle and tumor-to-blood radioactive uptake ratios are seen at 50 h p.i. (Fig. 5b, c and d); in accordance with imaging. The tumor-to-muscle reached 25 for OL in SSTr2-positive tumor as compared to 10 and 11.5 for CL in SSTr2- and control tumors, respectively. At 96 h, CL tumor-to-blood ratio of wild type tumor equalled that of OL for SSTr2-tumors reflecting degradation of LPs over time.

At the optimum imaging time point of 50 h p.i., PET-MR imaging co-registration allowed for clear tumor identification and demonstrates SSTr2 tumor specific contrast for OL (Fig. 6).

DISCUSSION

LPs are an established platform for drug and imaging agent delivery that exhibit low toxicity and biodegradability. In order to meet the demands of emerging multimodal hybrid molecular imaging, multifunctional targeted nanoparticles are proposed as single agent platforms. Herein, we described the synthesis, characterization and utility of a SSTr2-

targeting LP probe housing both a PET radionuclide (^{89}Zr) and a MR contrast agent (Gd-DTPA-bistearylamide).

OCT was successfully coupled to DSPE-PEG_{2000}-CO_2H and translated to LP conjugation, without the requirement of a protecting group. The notable difference in coupling yields between OCT reacted with lipid (7%) and OCT with LPs (70%) is attributed to the OCT adsorption to membranes (as previously reported) (29). We also observed the superior *in vitro* and *in vivo* tumor-targeting efficacy of OL in SSTr2-positive tumors over non-specific accumulation. No difference in liver and spleen uptake were observed between OL and CL, suggesting minimal peptide impact on LP surface.

The hypothesis of preformed LPs *direct-labeling* was first validated by observing Zr oxophilicity with lipid phosphate heads in a monolayer membrane. The radiolabeling strategy choice was influenced by the non-negligible DFO adsorption in the membranes. For instance, if a radiolabeling is conducted post DFO conjugation with LPs, it will result in ^{89}Zr-DFO desorption due to residual DFO adsorbed on the membranes. Consequently, this may lead to a dramatic decrease of the labeling efficiency. Instead, ^{89}Zr direct adsorption was chosen as a facile straightforward radiolabeling approach based on the supramolecular chemistry of ^{89}Zr with phospholipids.

Varying temperatures upon LP radiolabeling was informative of the radiolabeling mechanism. The high radiolabeling efficiency observed at 45°C indicated that the membrane fluidity played a critical role in ^{89}Zr adsorption. Higher temperatures correlated with a greater ^{89}Zr exchange through membranes, facilitating the penetration of ^{89}Zr within membranes. The radionuclide was likely entrapped in the LPs and then interacted with the luminal phosphates heads. Moreover, the concentration of LPs when radiolabeling seems to influence the radiolabeling efficiency. Low labeling efficiency associated with high lipid concentration suggested that LPs density in solution was an important factor of radiolabeling. High LP density is linked with low membranes accessibility due to hindrance between particles and therefore a substantial decrease of adsorptive radiolabeling was observed.

Analyzing the composition of ^{89}Zr-LPs, the ratio of lipid molecule number per trapped ^{89}Zr atom was found to be ~10^{12} lipid molecules per ^{89}Zr atom. The large number of lipid available for ^{89}Zr capture is likely to result in a permanent desorption / adsorption of ^{89}Zr within membranes, maintaining a stable traceable level of ^{89}Zr associated to liposomes. This may explain ^{89}Zr-LPs radioactive stability over serum protein challenge (50% ID from 24 to 96 h).

Unfortunately, serum protein studies and radioactive bone uptake suggested *in vitro* and *in vivo* limitations of this strategy regarding the radiolabeled LPs stability. It should however be noted that throughout this study the bone radioactivity never exceeded reported values of ^{89}Zr-DFO-monoclonal antibodies, 6 days p.i., in mice (~15% ID/g) (8). Furthermore, the presented LP radiolabeling method showed many advantages such as greatly simplifying the LPs formulation; reducing reaction time; and enhancing radiolabeling efficiency as well as quantitative tracking of long-circulating LPs. However, the stability of ^{89}Zr adsorbed LPs is debatable and an alternative LPs formulation using ^{89}Zr-DFO conjugate may decrease the short term bone uptake of free ^{89}Zr.

At 50 h p.i., the multifunctional LP construct resulted in the delivery of a high Gd payload at the disease sites providing significant enhancement in tumor contrast and high resolution of images; simultaneously, ^{89}Zr offered quantification of LP accumulation in targeted tissues. Tumor detection using PET was, however, difficult to interpret as compared to MR due to the hindrance of bone high signals, characteristic of ^{89}Zr release, and liver and spleen high

uptakes due to nanostructure biological fate. Nonetheless, at extended time point, 96 h p.i., LPs uptake in tumor tissue dropped to less than 2% ID/g corresponding to a Gd concentration inferior to 0.3 mM. Consequently, it involved a weaker detection of MR contrasts, as well as difficult and less accurate quantitative scans (30). Therefore, PET and MR imaging were complementary and necessary for this study to monitor LPs.

Despite limitations, both imaging methods were in good agreement, showing a 2-fold increase of agent uptake at 50 h p.i. for OL SSTr2-positive tumor compared to CL. This observation correlates with PEG_{2000}-LPs pharmacology, where the optimum tumor uptake is reported to be 48 h p.i (9). Although non-specific EPR effect was seen, PET/MR dual detection clearly highlighted OL tumor-specificity over CL. This proof-of-concept imaging approach may be an interesting application to translate for the tracking and quantification of clinical drug-LPs.

CONCLUSION

In conclusion, we achieved and characterized the formulation of a novel SSTr2-targeting PET/MR LP and assessed *in vitro* and *in vivo* specific SSTr2 recognition through OCT conjugated LPs. A direct ^{89}Zr-radiolabeling method of preformed LPs was described and its imaging applicability as a long circulating dual PET-MR tacking probe was demonstrated. Having established this methodology, other tumor-targeting moieties can be associated to LPs. It is conceivable that this PET-MR LP formulation could image the biological behaviour of LP-based drugs, enabling early prediction of therapy response.

Supplementary Material

Refer to Web version on PubMed Central for supplementary material.

Acknowledgments

DISCLOSURES

This work was funded in part by the Geoffrey Beene Cancer Research Center of MSKCC (JSL), the Office of Science (BER) - U.S. Department of Energy (Award DE-SC0002456; JSL). We thank Drs. Grimm, Blasberg, Pillarsetty, McDevitt and Le for their insights. We also acknowledge support provided by Mr. William H., Mrs. Alice Goodwin, the Commonwealth Foundation for Cancer Research and The Experimental Therapeutics Center of Memorial Sloan-Kettering Cancer Center. Finally, we would like to thank technical services provided by the MSKCC Small-Animal Imaging Core Facility.

References

1. Cherry SR. Multimodality imaging: beyond PET/CT and SPECT/CT. Semin Nucl Med. 2009; 39(5):348–53. Epub 2009/08/04. [PubMed: 19646559]
2. Catana C, Procissi D, Wu Y, Judenhofer MS, Qi J, Pichler BJ, et al. Simultaneous *in vivo* positron emission tomography and magnetic resonance imaging. Proc Natl Acad Sci U S A. 2008; 105(10): 3705–10. Epub 2008/03/06. [PubMed: 18319342]
3. Bellin MF. MR contrast agents, the old and the new. Eur J Radiol. 2006; 60(3):314–23. Epub 2006/09/29. [PubMed: 17005349]
4. Shellock FG. MR imaging in patients with intraspinal bullets. J Magn Reson Imaging. 1999; 10(1): 107. Epub 1999/07/10. [PubMed: 10398986]
5. Terreno E, Delli Castelli D, Cabella C, Dastru W, Sanino A, Stancanello J, et al. Paramagnetic liposomes as innovative contrast agents for magnetic resonance (MR) molecular imaging applications. Chem Biodivers. 2008; 5(10):1901–12. Epub 2008/10/31. [PubMed: 18972531]
6. Soret M, Bacharach SL, Buvat I. Partial-volume effect in PET tumor imaging. J Nucl Med. 2007; 48(6):932–45. Epub 2007/05/17. [PubMed: 17504879]

7. Phillips WT, Goins BA, Bao A. Radioactive liposomes. Wiley Interdiscip Rev Nanomed Nanobiotechnol. 2009; 1(1):69–83. Epub 2010/01/06. [PubMed: 20049780]
8. Holland JP, Divilov V, Bander NH, Smith-Jones PM, Larson SM, Lewis JS. 89Zr-DFO-J591 for immunoPET of prostate-specific membrane antigen expression *in vivo*. J Nucl Med. 2010; 51(8): 1293–300. Epub 2010/07/28. [PubMed: 20660376]
9. Laverman P, Boerman OC, Oyen WJG, Corstens FHM, Storm G. *In vivo* applications of PEG liposomes: unexpected observations. Crit Rev Ther Drug Carrier Syst. 2001; 18(6):551–66. Epub 2002/ 01/16. [PubMed: 11789675]
10. ElBayoumi TA, Torchilin VP. Tumor-targeted nanomedicines: enhanced antitumor efficacy *in vivo* of doxorubicin-loaded, long-circulating liposomes modified with cancer-specific monoclonal antibody. Clin Cancer Res. 2009; 15(6):1973–80. Epub 2009/03/12. [PubMed: 19276264]
11. Iwase Y, Maitani Y. Octreotide-targeted liposomes loaded with CPT-11 enhanced cytotoxicity for the treatment of medullary thyroid carcinoma. Mol Pharm. 2011; 8(2):330–7. Epub 2010/12/21. [PubMed: 21166471]
12. Iwase Y, Maitani Y. Dual functional octreotide-modified liposomal irinotecan leads to high therapeutic efficacy for medullary thyroid carcinoma xenografts. Cancer Sci. 2012; 103(2):310–6. [PubMed: 22017398]
13. Reubi JC. Peptide receptors as molecular targets for cancer diagnosis and therapy. Endocr Rev. 2003; 24(4):389–427. Epub 2003/08/16. [PubMed: 12920149]
14. Sun M, Wang Y, Shen J, Xiao Y, Su Z, Ping Q. Octreotide-modification enhances the delivery and targeting of doxorubicin-loaded liposomes to somatostatin receptors expressing tumor in vitro and *in vivo*. Nanotechnology. 2010; 21(47):475101. Epub 2010/10/30. [PubMed: 21030757]
15. Holland JP, Sheh Y, Lewis JS. Standardized methods for the production of high specific-activity zirconium-89. Nucl Med Biol. 2009; 36(7):729–39. Epub 2009/09/02. [PubMed: 19720285]
16. Stewart JC. Colorimetric determination of phospholipids with ammonium ferrothiocyanate. Anal Biochem. 1980; 104(1):10–4. Epub 1980/05/01. [PubMed: 6892980]
17. Medina OP, Pillarsetty N, Glekas A, Punzalan B, Longo V, Gonen M, et al. Optimizing tumor targeting of the lipophilic EGFR-binding radiotracer SKI 243 using a liposomal nanoparticle delivery system. J Control Release. 2011; 149(3):292–8. Epub 2010/11/05. [PubMed: 21047536]
18. Barlow DJ, Hollinshead CM, Harvey RD, Webster JRP, Hughes AV, Weston A, et al. Effects of surface pressure on the structure of distearoylphosphatidylcholine monolayers formed at the air/ water interface. Langmuir. 2009; 25(7):4070–7. [PubMed: 19714892]
19. Abou DS, Ku T, Smith-Jones PM. *In vivo* biodistribution and accumulation of 89Zr in mice. Nucl Med Biol. 2011; 38(5):675–81. Epub 2011/07/02. [PubMed: 21718943]
20. Enoch HG, Strittmatter P. Formation and properties of 1000-A-diameter, single-bilayer phospholipid vesicles. Proc Natl Acad Sci U S A. 1979; 76(1):145–9. Epub 1979/01/01. [PubMed: 34148]
21. Zhang H, Moroz MA, Serganova I, Ku T, Huang R, Vider J, et al. Imaging expression of the human somatostatin receptor subtype-2 reporter gene with 68 Ga-DOTATOC. J Nucl Med. 2011; 52(1):123–31. Epub 2010/12/15. [PubMed: 21149478]
22. Euhus DM, Hudd C, LaRegina MC, Johnson FE. Tumor measurement in the nude mouse. J Surg Oncol. 1986; 31(4):229–34. Epub 1986/04/01. [PubMed: 3724177]
23. Beattie BJ, Forster GJ, Govantes R, Le CH, Longo VA, Zanzonico PB, et al. Multimodality registration without a dedicated multimodality scanner. Mol Imaging. 2007; 6(2):108–20. Epub 2007/04/21. [PubMed: 17445505]
24. Na DH, Murty SB, Lee KC, Thanoo BC, DeLuca PP. Preparation and stability of poly(ethylene glycol) (PEG)ylated octreotide for application to microsphere delivery. AAPS PharmSciTech. 2003; 4(4):E72. Epub 2004/06/17. [PubMed: 15198567]
25. Strijkers GJ, Mulder WJ, van Heeswijk RB, Frederik PM, Bomans P, Magusin PC, et al. Relaxivity of liposomal paramagnetic MRI contrast agents. MAGMA. 2005; 18(4):186–92. Epub 2005/09/13. [PubMed: 16155762]
26. Dijkers EC, Oude Munnink TH, Kosterink JG, Brouwers AH, Jager PL, de Jong JR, et al. Biodistribution of 89Zr-trastuzumab and PET imaging of HER2-positive lesions in patients with

meta-static breast cancer. Clin Pharmacol Ther. 2010; 87(5):586–92. Epub 2010/04/02. [PubMed: 20357763]

27. Fabre RM, Talham DR. Stable supported lipid bilayers on zirconium phosphonate surfaces. Langmuir. 2009; 25(21):12644–52. Epub 2009/08/29. [PubMed: 19711922]
28. Maeda H, Wu J, Sawa T, Matsumura Y, Hori K. Tumor vascular permeability and the EPR effect in macromolecular therapeutics: a review. J Control Release. 2000; 65(1–2):271–84. Epub 2000/03/04. [PubMed: 10699287]
29. Beschiaschvili G, Seelig J. Peptide binding to lipid bilayers. Nonclassical hydrophobic effect and membrane-induced pK shifts. Biochemistry. 1992; 31(41):10044–53. Epub 1992/10/20. [PubMed: 1390763]
30. Ahrens ET, Rothbacher U, Jacobs RE, Fraser SE. A model for MRI contrast enhancement using T1 agents. Proc Natl Acad Sci U S A. 1998; 95(15):8443–8. Epub 1998/07/22. [PubMed: 9671697]

ABBREVIATIONS

CL	control-liposome
CT	computed tomography
LP	liposome
MRI	magnetic resonnance imaging
OCT	octreotide
OL	octreotide-liposome
PEG	polyethylene glycol
PET	positron emission tomography
SPECT	single-photon emission computed tomography
SSTr2	somatostatin receptor subtype 2

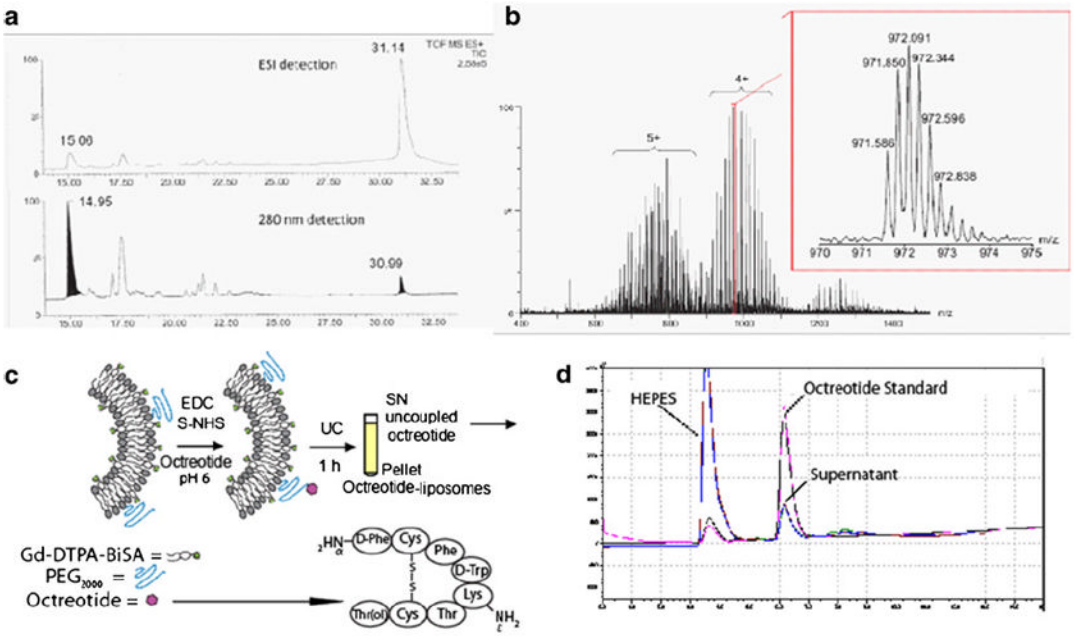

Fig. 1.

Characterization of OCT coupled to DSPE-PEG_{2000}-CO_2H (**a** and **b**) and to LPs (**c** and **d**). (**a**) C4-HPLC chromatogram of OCT and DSPE-PEG_{2000}-CO_2H coupling performed at pH 6 with EDC and S-NHS and acquired using electrospray ionization-QTOF-MS (ESI) and UV-280 nm detection. (**b**) Mass spectrum of mono-coupled DSPE-PEG_{2000}-N-OCT, eluted at 31 min (chromatogram A). (**c**) OL conjugation scheme starting with Gd-CL; UC: ultracentrifugation. (**d**) HPLC evaluation of coupling efficiency by subtracting post-reaction supernatant (SN) OCT concentration from the initial OCT reaction concentration.

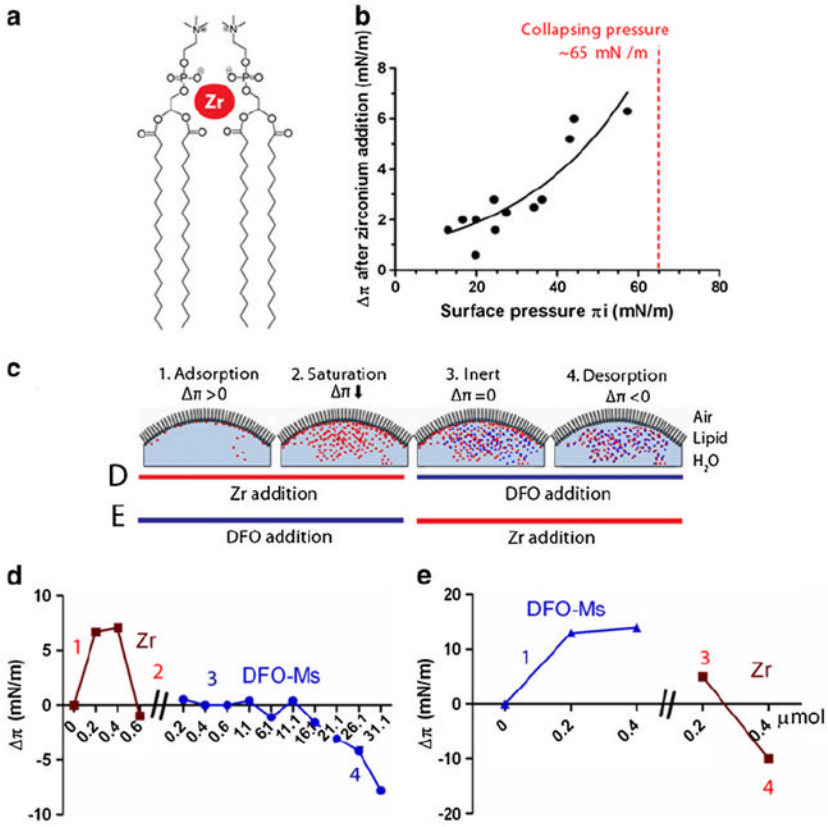

Fig. 2.

Direct Zr adsorption on lipid membranes. (**a**) Scheme of Zr binding to adjacent lipidic phosphate heads. (**b**) The surface tension $\Delta\pi$ increases upon addition of Zr (0.2 μmol) at various initial surface pressures (π_i). (**c**) Scheme of DSPC monolayer membrane states (#1 to #4) characterized by $\Delta\pi$ variation. $\Delta\pi$ is: #1) positive and increasing when lipids adsorb substrates (Zr, red, or DFO, blue); #2) dropped when the membrane saturates in adsorbing substances; #3) stable when no interaction occurs with the membrane; and, #4) negative and decreasing when Zr-DFO complexes desorb from the membrane. (**d** and **e**) $\Delta\pi$ variation upon adsorption of Zr (red line) or DFO (blue line), followed by Zr-DFO desorption upon the addition of DFO or Zr.

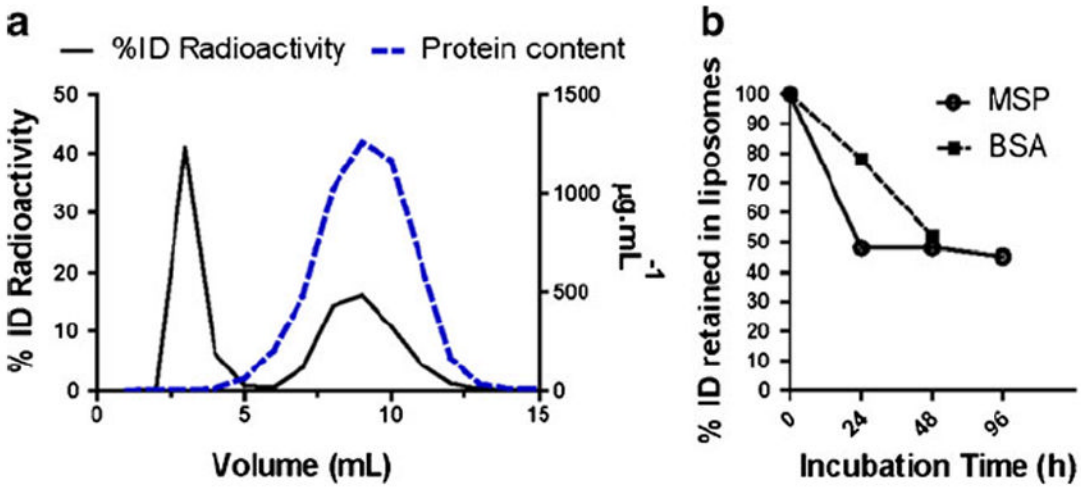

Fig. 3.

Stability study of ^{89}Zr-LPs. (**a**) Size exclusion chromatogram of the 48 h incubated mixture: mouse serum protein (MSP) and ^{89}Zr-LPs. (**b**) LPs radioactivity stability profile after incubation and purification at 24; 48; 96 h with MSP or BSA (5%w/v); $n \geq 2$.

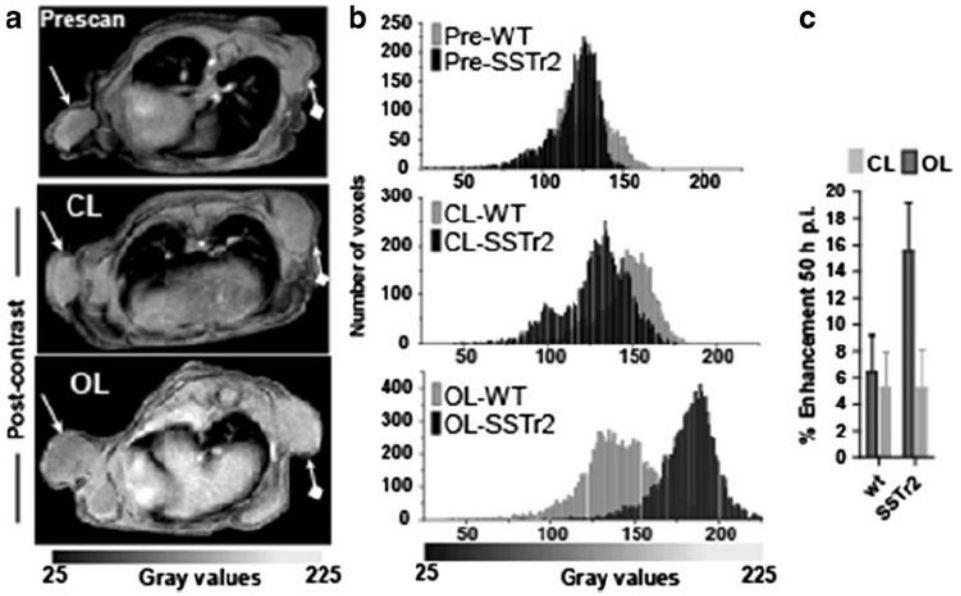

Fig. 4.

(**a**) 50 h p.i. T_1-weighted MR scan of mice implanted with wild type (wt) (→) and SSTr2-postive tumors (◆→), injected with OL and CL (35–40 μCi; 18.5 mM–2.78 μmol Gd-DTPA-BiSA; 43.5 mM–6.53 μmol lipids). (**b**) Voxel-wise analysis of tumors normalized (to standard) intensity. Selective MR enhancement is achieved using targeted OL. (**c**) Percentage of contrast enhancement (prescan to 50 h p.i.) of tumor ROI normalized to water standard. Nearly two fold enhancement is observed using targeted OL (n=5; SEM).

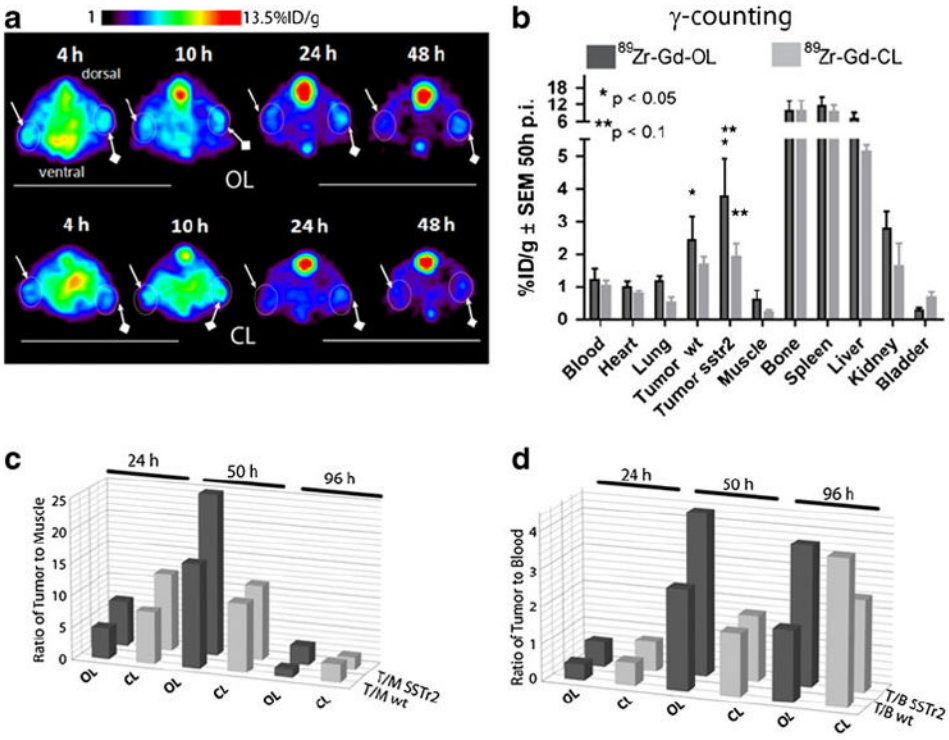

Fig. 5.

(**a**) Axial PET slices, acquired at 4, 10, 24, 48 h p.i. of mice bearing wild type (wt) (→) and SSTr2-postive tumors (◆→) and injected with OL (top row) and CL (bottom), the bright spot corresponds to the spine. (**b**) 50 h p.i. radioactivity distribution following administration of OL and CL (*n*=5; SEM). (**c** and **d**) Radioactive tumor-to-muscle and tumor-to-blood ratios for each LP group at 24, 50 and 96 h.

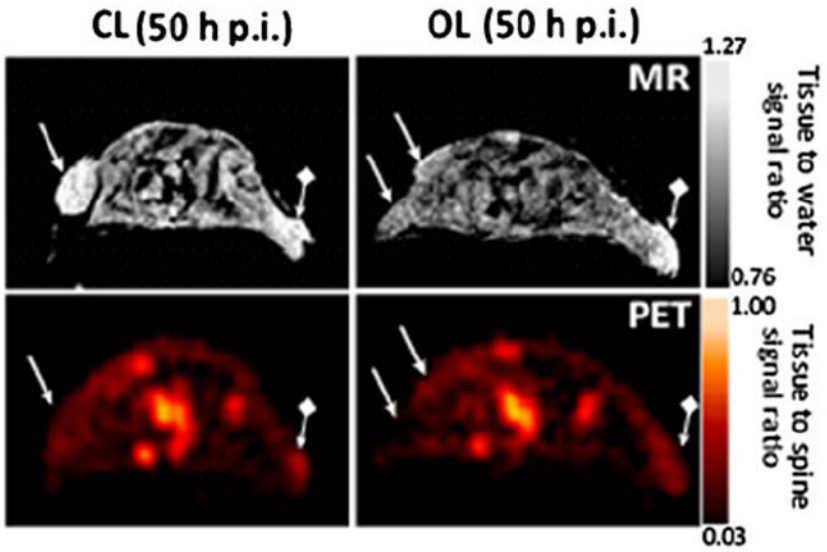

Fig. 6.

PET/MR co-registration: MR (top row) and PET (bottom) scans of mice bearing wild type (wt) (→) and SSTr2-postive tumors (◆→) and injected with CL (left panel) and OL (right panel).

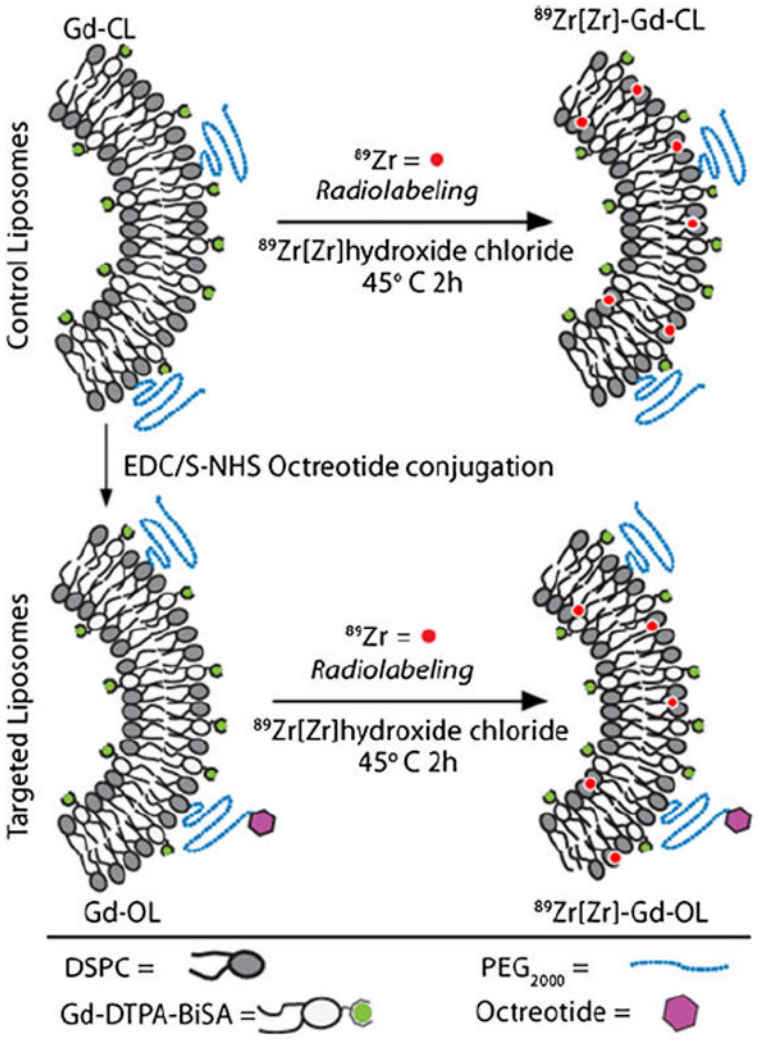

Scheme 1.

LP constructs and radiolabeling strategy: OCT was conjugated to preformed Gd-Control LPs (CL) resulting in targeted OCT-LP (OL). Both paramagnetic formulations were radiolabeled using ^{89}Zr with a chelator-free approach.